

# Boronization of Nickel Foam for Sustainable Electrochemical Reduction of Nitrate to Ammonia

Zhong-Hua Xue,<sup>†</sup> Han-Cheng Shen,<sup>†</sup> Peirong Chen, Guang-Xue Pan, Wei-Wei Zhang, Wei-Meng Zhang, Shi-Nan Zhang, Xin-Hao Li,\* and Cafer T. Yavuz\*



Cite This: *ACS Energy Lett.* 2023, 8, 3843–3851



Read Online

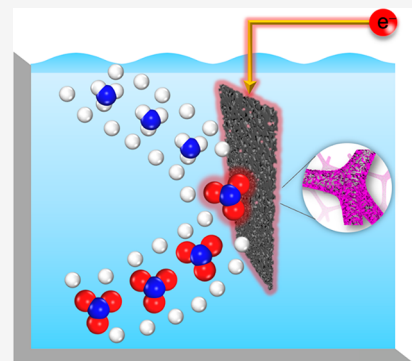
ACCESS |

Metrics & More

Article Recommendations

Supporting Information

**ABSTRACT:** Electrochemical reduction of aqueous nitrates has emerged as a sustainable and practical approach in combining water treatment and ammonia fertilizer synthesis. However, the development of highly integrated catalytic electrodes with consistently high activity from non-noble metals remains a challenging issue despite the potential to greatly decrease costs and promote real-world applications. Here, we report a high-performance electrode with electron-abundant surfaces obtained from direct boronization of nickel foam, rendering a stable ammonia yield rate of  $19.2 \text{ mg h}^{-1} \text{ cm}^{-2}$  with high Faradaic efficiency of 94% for  $\text{NO}_3^-$ -to- $\text{NH}_3$  conversion. The microprocessing lowers the work function and initiates a local electric field for the nickel foam by converting acid-stable surface nickel oxides into dyadic nanosheets composed of metallic nickel and amorphous nickel borates, thus promoting the adsorption and transformation of nitrate anions. Furthermore, the spent electrode enables a rapid and effective regeneration by undergoing another round of boronization, which ensures a long lifetime for the practical application of our electrode design.



Nitrate ( $\text{NO}_3^-$ ), the most oxidized form of nitrogen, is widely present on earth, and its increased production for the purpose of fertilizers and explosives has cascading adverse effects on the environment and poses significant health risks such as methemoglobinemia and cancer.<sup>1–6</sup> Finding effective ways to convert the nitrate into harmless  $\text{N}_2$  or value-added  $\text{NH}_3$  for agriculture and industry is, therefore, crucial.<sup>7–11</sup> Electrochemical approaches have emerged as promising solutions in achieving this goal, especially by utilizing excess and discrete sustainable electricity.<sup>12–16</sup> Notably, the electrochemical reduction of nitrate to ammonia has been demonstrated as a viable conversion method for mitigating water pollution and, simultaneously, large-scale  $\text{NH}_3$  production.<sup>14,17,18</sup> However, this reaction requires an efficient heterogeneous catalyst or a catalytic electrode to selectively accelerate the eight-electron and nine-proton reaction.<sup>17,19,20</sup> While noble-metal-based materials, particularly those containing Ru, have been shown to be effective in facilitating the selective transformation of  $\text{NO}_3^-$  into  $\text{NH}_3$  with decent efficiencies,<sup>14,21–26</sup> their scarcity and high costs hinder their widespread application. Thus, developing cost-competitive catalysts based on earth-abundant transition metals is of tremendous interest for the practical application of electrochemical  $\text{NO}_3^-$ -to- $\text{NH}_3$  conversion.<sup>8,13,27–31</sup>

Nitrate presents a unique challenge for metal catalysts due to weaker nucleophilicity and consequently lower binding affinity onto the catalyst surfaces when compared to other common ions like  $\text{H}_3\text{O}^+$ .<sup>32,33</sup> In principle, controlled binding of  $\text{H}_3\text{O}^+$  on metal centers is required to provide sufficient protons for the nitrate hydrogeneration but at the same time to depress the kinetics of hydrogen evolution reaction (HER), thereby achieving a rapid  $\text{NH}_3$  yield rate with improved selectivity measured by Faradaic efficiencies (FEs).<sup>33,34</sup> However, non-noble metal based catalysts still suffer from low performance for  $\text{NO}_3^-$ -to- $\text{NH}_3$  conversion due to the imperfect electronic and surface structures. For example, Cu-based electrocatalysts have weak adsorption of both nitrate and protons, resulting in decreased activity and stability due to the surface poisoning.<sup>35</sup> Conversely, cheaper Ni electrocatalysts exhibit strong adsorption of protons leading to decreased FEs for  $\text{NH}_3$  due to its relatively high work function.<sup>36,37</sup> Hence, it is necessary

Received: June 8, 2023

Accepted: August 2, 2023

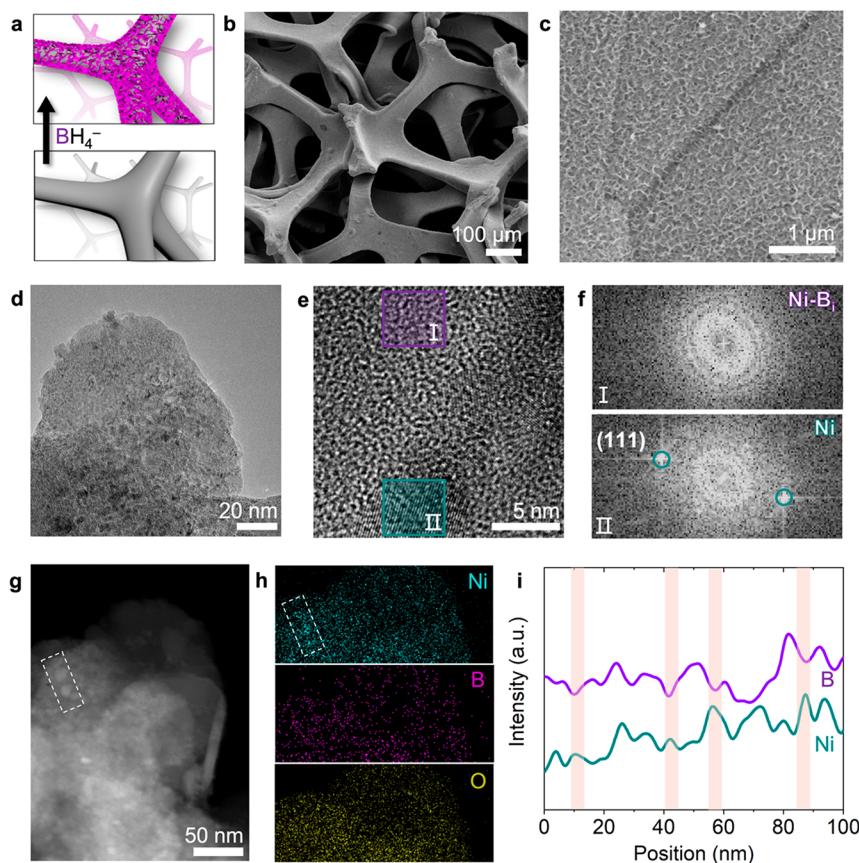


**Figure 1.** Fabrication and structure of  $\text{Ni-BO}_x/\text{NF}$  electrode. (a) Synthetic process. (b and c) SEM images of  $\text{Ni-BO}_x/\text{NF}$  electrode. (d) TEM image and HRTEM image (e) of surface  $\text{Ni-BO}_x$  nanosheets and corresponding FFT images (f) taken from marked areas of frame I and II in panel e. (g) HAADF-TEM image and corresponding EDX elemental mapping (h) of surface  $\text{Ni-BO}_x$  nanosheets; scale bar in panel h: 50 nm. (i) EDX line scanning along the nanosheets in Figure S8a.

to develop a specific metal surface with targeted electronic structure for efficient and selective reduction of  $\text{NO}_3^-$  into  $\text{NH}_3$ .<sup>36,38–42</sup> In addition, developing inexpensive electrodes is essential to make electrochemical nitrate reduction more deployable,<sup>43</sup> but this remains elusive.

Here, we report a simple strategy for modifying a metal surface to tune its electron-donor capacity to achieve high-efficiency reduction of nitrate to ammonia. Our facile and effective approach involves immersing a bare nickel foam (NF) in a sodium borohydride ( $\text{NaBH}_4$ ) solution to form dyadic nanosheets on its surface. The as-formed nanosheets, composed of metallic nickel and amorphous nickel borate ( $\text{Ni-BO}_x$ ), lower the work function of NF, making the resultant  $\text{Ni-BO}_x/\text{NF}$  electrode surface electron-abundant. When tested in practical conditions, the electron-rich  $\text{Ni-BO}_x/\text{NF}$  demonstrated a rapid ammonia yield rate of over  $19.2 \text{ mg h}^{-1} \text{ cm}^{-2}$  with a high FE of over 94%, significantly upgrading the performance of raw NF for electrochemical  $\text{NO}_3^-$ -to- $\text{NH}_3$ . The spent  $\text{Ni-BO}_x/\text{NF}$  electrode could be recycled easily and quickly by applying a repetitive boronization process. Our theoretical calculations combined with an electrochemical *in situ* external reflection Fourier transform infrared (FTIR) spectroscopy revealed that the elevated  $\text{NO}_3^-$ -to- $\text{NH}_3$  activity over an electron-abundant Ni surface resulted from lowering the barrier of the potential-dependent step (PDS), enhancing the adsorption energy of the nitrate anion, and depressing the HER.

**Fabrication and Characterization of  $\text{Ni-BO}_x/\text{NF}$ .** The  $\text{Ni-BO}_x/\text{NF}$  electrode was fabricated by direct immersion of a cleaned NF in  $\text{NaBH}_4$  solution at room temperature (Figure 1a; methods are in the Supporting Information). Scanning electron microscopy (SEM) images clearly show the foamy scaffold of the electrode and the uniform formation of nanosheets onto the bare NF surfaces by virtue of the mild boronization process (Figures 1b,c, S1, and S2). Transmission electron microscopy (TEM) provides more details about the as-formed nanosheets (Figures 1d and S3). High-resolution TEM (HRTEM) and the corresponding fast Fourier transform (FFT) observations (Figures 1e,f and S4) reveal that the nanosheets are uniquely composed of both amorphous nickel borate ( $\text{Ni-B}_i$ , as also demonstrated by a subsequent elemental analysis) and crystalline metallic nickel phase.<sup>44,45</sup> HRTEM images (Figure S5) and selected area electron diffraction (SAED) patterns (Figure S6) further confirm the generation of an amorphous/crystalline matrix and the trace existence of crystalline nickel borate ( $\text{Ni}_3(\text{BO}_3)_2$ ) inside the nanosheets. Moreover, high-angle annular dark-field TEM (HAADF-TEM) images (Figure 1g) and the related energy dispersive X-ray spectroscopy (EDX) elemental mapping results (Figures 1h and S7) indicate the distribution of Ni/B/O atoms and that some metallic Ni nanoclusters are clearly visible (the dotted box) along the nanosheets. The EDX line spectrum confirms a differential distribution between B and Ni (Figures 1i and S8), disclosing the decoration of Ni nanoclusters on amorphous  $\text{Ni-B}_i$ .

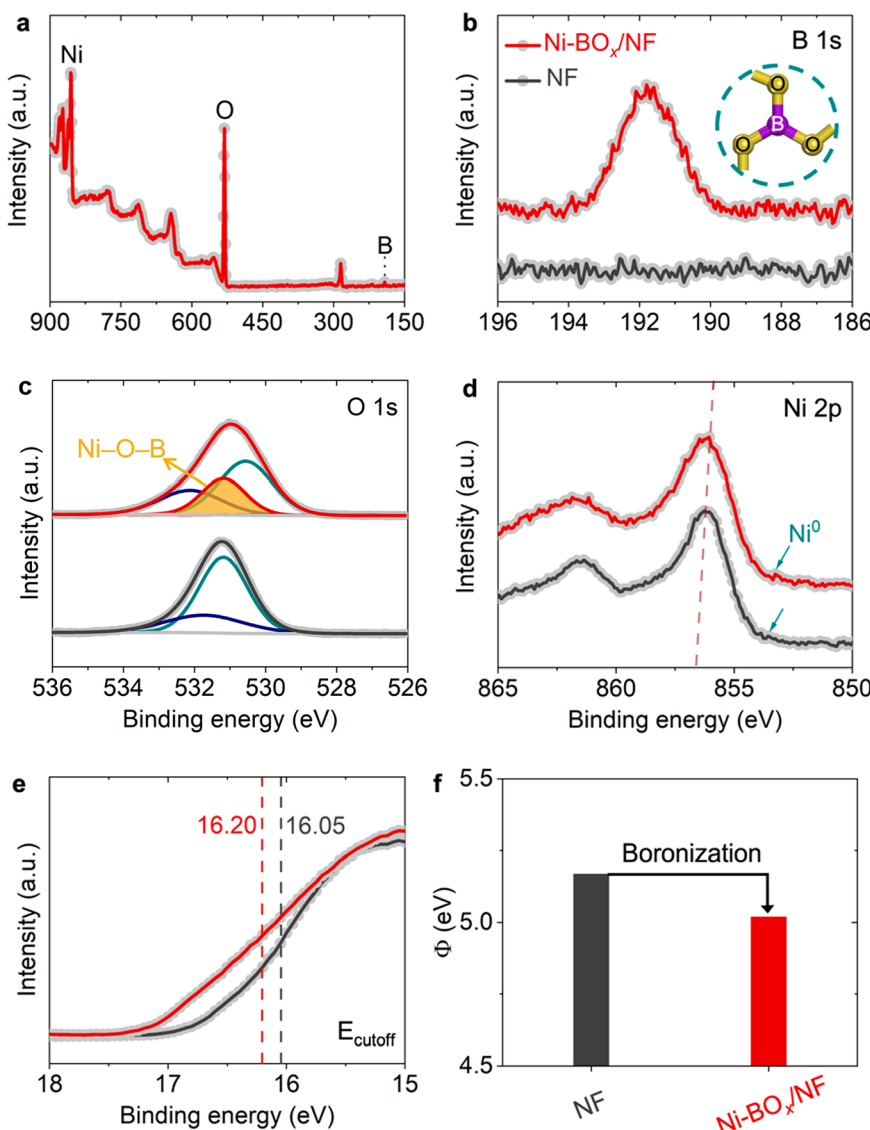


**Figure 2.** Electronic structure analysis of the electrodes. (a) XPS survey scan, high-resolution XPS B 1s (b), O 1s (c), and (d) Ni 2p spectra. The inset of panel b shows the structure of borate species. (e) UPS spectra in the secondary electron cutoff energy region and (f) measured work functions of  $\text{Ni-BO}_x/\text{NF}$  and NF electrodes.

The X-ray diffraction (XRD) pattern of  $\text{Ni-BO}_x/\text{NF}$  exhibits only the peaks indexed to the metallic nickel without those of the crystalline nickel borate phase,<sup>45</sup> further indicating that the  $\text{Ni-B}_i$  species are mainly amorphous (Figure S9). According to these results, we can envision that our strategy is primarily a surface boronization process of acid-stable nickel oxide on the surface of NF ( $4\text{NiO(s)} + 2\text{BH}_4^-(\text{aq}) + 4\text{H}_2\text{O(l)} \rightarrow \text{Ni(s)} + \text{Ni}_3(\text{BO}_3)_2(\text{s}) + 7\text{H}_2(\text{g}) + 2\text{OH}^-(\text{aq})$ ).<sup>46</sup>

**Identification of Electron-Abundant Ni Surface.** We employed X-ray and ultraviolet photoelectron spectroscopy (XPS/UPS) to analyze the surface components and electronic structure of the  $\text{Ni-BO}_x/\text{NF}$  electrode in detail. Based on the XPS elemental scan results (Figure 2a) and also combined with the above TEM observations (Figures S5 and S6), the surface atomic B/O ratio of  $\text{Ni-BO}_x/\text{NF}$  is ca. 1:4.7, allowing the amorphous  $\text{Ni-B}_i$  phase to be approximately formulated as  $\text{Ni}_3(\text{BO}_3)_2$ , excluding the surface-absorbed oxygen.<sup>47</sup> The high-resolution B 1s spectrum shows a characteristic peak at 191.8 eV after the boronization (Figure 2b), which is attributed to the core levels of  $\text{B}^{3+}$  in nickel borate species.<sup>48</sup> In the O

regions (Figure 2c), we can observe the binding energies vested in the Ni–O (530.7 eV), nascent Ni–O–B (531.4 eV), and adsorbed O (532.4 eV).<sup>49</sup> Typical Ni 2p spectra reveal that the peaks of Ni species shift to lower binding energy values, and the  $\text{Ni}^0$  signal (~853.5 eV) becomes much more significant as NF is transferred to  $\text{Ni-BO}_x/\text{NF}$  (Figures 2d and S10),<sup>44</sup> attributed to the surface reduction of NF and the electron transfer from B to O.<sup>33</sup> This supports the mechanism of the boronization process, leading to the decrease of nickel oxidation state for  $\text{Ni-BO}_x/\text{NF}$ . As analyzed by UPS spectra (Figures 2e,f and S11), the  $\text{Ni-BO}_x/\text{NF}$  electrode exhibited a measured work function ( $\Phi$ ) of 5.02 eV, which is lower than that of NF (5.17 eV).<sup>16,44</sup> All of these results indicate the successful formation of the electron-abundant Ni surface by a simple boronization treatment. The electron-abundant Ni surface with lowered work function thus offers the  $\text{Ni-BO}_x/\text{NF}$  electrode balanced ability to depress the hydrogen evolution reaction and accelerate the eight-electron hydrogenation of nitrate into ammonia.<sup>36</sup>

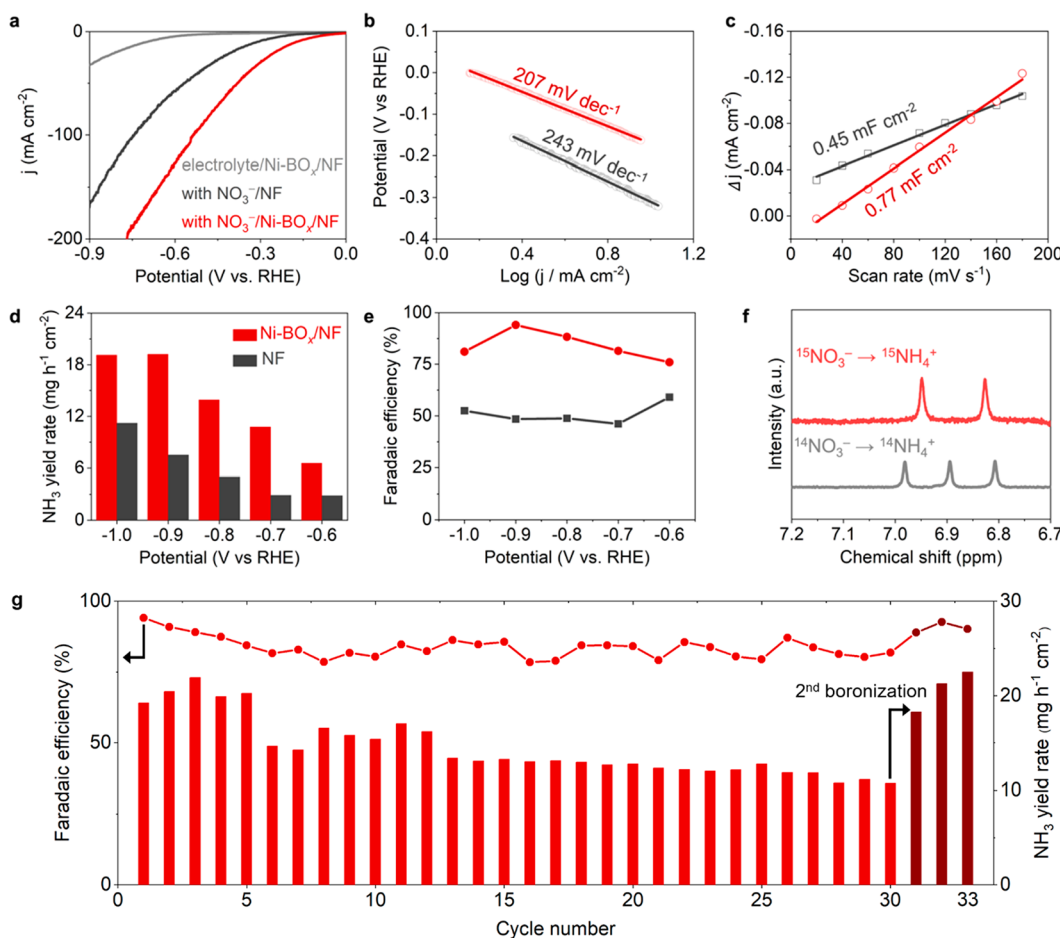


**Figure 3.** Electrocatalytic performance of nitrate reduction into ammonia. (a) LSV curves in electrolyte with and without addition of 0.50 M  $\text{NaNO}_3$  (scan rate: 10  $\text{mV s}^{-1}$ ), (b) corresponding Tafel plots, (c)  $C_{dl}$  measurements, potential-dependent  $\text{NH}_3$  yield rate (d), and FEs (e) over the NF and  $\text{Ni-BO}_x/\text{NF}$  electrodes. (f)  $^1\text{H}$  NMR spectra of the electrolyte on  $\text{Ni-BO}_x/\text{NF}$  electrode using  $^{14}\text{NO}_3^-$  and  $^{15}\text{NO}_3^-$  as the nitrate source. (g) Recycling test at potential of -0.9 V vs RHE for  $\text{Ni-BO}_x/\text{NF}$  electrode.

**Table 1. Comparison of Electrochemical  $\text{NO}_3^-$ -to- $\text{NH}_3$  Performances of the  $\text{Ni-BO}_x/\text{NF}$  Electrode with Reported Catalysts**

Catalyst	Electrolyte	Highest $\text{NH}_3$ yield rate ( $\text{mg h}^{-1} \text{cm}^{-2}$ )	Highest FE (%)	Reference
$\text{Ni-BO}_x/\text{NF}$	0.1 M $\text{Na}_2\text{SO}_4$ + 0.5 M $\text{NaNO}_3$	22.5	94	This work
$\text{Ni}_3\text{B@NiB}_{2.74}$	0.10 M KOH + 100 mM $\text{KNO}_3$	3.4	~100	33
$\text{Ni}_{35}/\text{NC-sd}$	0.5 M $\text{Na}_2\text{SO}_4$ + 0.3 M $\text{NaNO}_3$	5.1	99	8
$\text{BCN@Ni}$	0.10 M KOH + 100 mM $\text{KNO}_3$	2.3	91.1	18
$\text{Ni}_1\text{Cu-SAA}$	0.5 M $\text{K}_2\text{SO}_4$ + 200 ppm $\text{KNO}_3$	5.6	~100	19
$\text{Fe}/\text{Ni}_2\text{P}$	0.2 M $\text{K}_2\text{SO}_4$ + 0.05 M $\text{KNO}_3$	4.2	94.3	29
$\text{RM} (\text{Fe}_2\text{O}_3+\text{Al}_x\text{Si}_y\text{O}_z)$	1 M PBS + 1 M $\text{KNO}_3$	2.7	92.8	30
$\text{BiFeO}_3$	0.1 M KOH + 0.1 M $\text{KNO}_3$	~10.2	96.9	50
$\text{Fe}_3\text{O}_4/\text{SS}$	0.1 M NaOH + 0.1 M $\text{NaNO}_3$	10.1	91.5	31
$\text{Fe SAC}$	0.1 M $\text{K}_2\text{SO}_4$ + 0.5 M $\text{KNO}_3$	7.8	~75	27
$\text{Co-Fe@Fe}_2\text{O}_3$	0.1 M $\text{Na}_2\text{SO}_4$ + 1000 ppm of $\text{NaNO}_3$	1.5	85.8	51
$\text{Co-CNP}$	0.02 M $\text{Na}_2\text{SO}_4$ + 100 mg/L $\text{NaNO}_3$	0.4	92	28
$\text{O-Cu-PTCDA}$	0.1 M PBS + 500 ppm $\text{KNO}_3$	0.5	85.9	13
$\text{Cu-N-C}$	0.1 M KOH + 0.1 M $\text{KNO}_3$	4.5	84.7	39
$\text{Poly-Cu}_{14}\text{cba}$	0.5 M $\text{K}_2\text{SO}_4$ + 250 ppm $\text{KNO}_3$	2.8	90	52
$\text{Pd-NDs/Zr-MOF}$	0.1 M $\text{Na}_2\text{SO}_4$ + 500 ppm of $\text{NaNO}_3$	2.0	58.1	24
$\text{Pd/TiO}_2$	1 M LiCl + 0.25 M $\text{LiNO}_3$	1.1	92.1	23
$\text{Cu/Pd/CuO}_x$	0.5 M $\text{K}_2\text{SO}_4$ + 50 mg/L $\text{KNO}_3$	3.0	84	53
$\text{CuCoSP}$	0.1 M KOH + 0.1 M $\text{KNO}_3$	19.9	93.3	15
Ru nanoclusters	1 M KOH + 1 M $\text{KNO}_3$	19.9	~100	21
$\text{Rh@Cu-0.6\%}$	0.1 M $\text{Na}_2\text{SO}_4$ + 0.1 M $\text{KNO}_3$	21.6	93	22

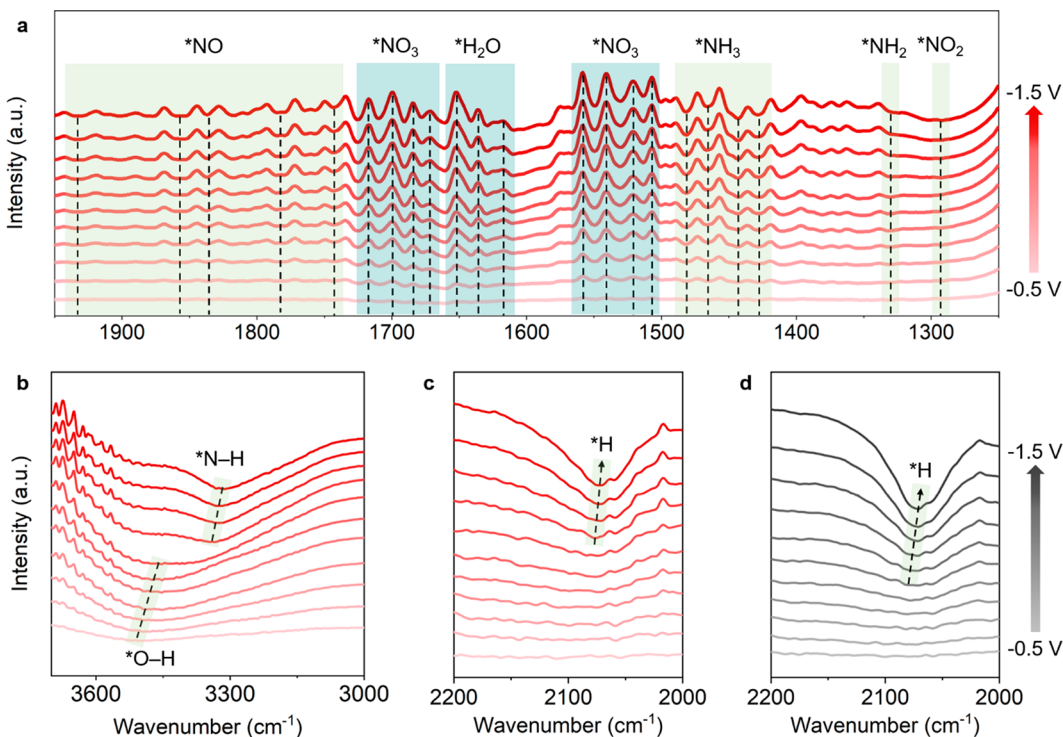


**Figure 4.** Potential-dependent *in situ* external reflection FTIR spectra. Spectra on Ni-BO<sub>x</sub>/NF (a–c) and NF (d) electrodes in electrolyte of 0.1 M Na<sub>2</sub>SO<sub>4</sub> + 0.5 M NaNO<sub>3</sub> from −0.5 to −1.5 V (vs RHE).

**Catalytic Performance of Electrodes.** We measured the catalytic performance of the Ni-BO<sub>x</sub>/NF electrodes for nitrate reduction over a standard three-electrode system (see the methods in the Supporting Information). The increased current density in the linear sweep voltammogram (LSV) curves of the NF after the inclusion of 0.5 M NaNO<sub>3</sub> verifies the electrocatalytic activity for NO<sub>3</sub><sup>−</sup> reduction (Figure 3a). The Ni-BO<sub>x</sub>/NF electrode further lowers the potential and presents a smaller Tafel slope (Figure 3a,b), proving better activity and corresponding to faster reaction kinetics than NF. Furthermore, the calculation of electrochemically active surface area (ECSA) based on double-layer capacitance ( $C_{dl}$ ) tests (Figures 3c and S12) indicates that the Ni-BO<sub>x</sub>/NF (1.0 cm<sup>2</sup> ECSA) exhibits a higher ECSA than NF (1.7 cm<sup>2</sup> ECSA), attesting to the elevated intrinsic activity toward nitrate reduction by the surface boronization.<sup>14,27</sup>

We evaluated the yields of NH<sub>3</sub> and FEs by a colorimetric indophenol blue method (Figure S13) and confirmed this with <sup>1</sup>H nuclear magnetic resonance (<sup>1</sup>H NMR) analysis (Figure S14). Upon increasing the applied potential (Figures 3d and S15), the Ni-BO<sub>x</sub>/NF rendered a maximum NH<sub>3</sub> yield rate of 19.2 mg h<sup>−1</sup> cm<sup>−2</sup> at −0.9 V vs RHE by a high current density output of more than −200 mA cm<sup>−2</sup>, outpacing NF by more than 2.55 times. The FEs toward NO<sub>3</sub><sup>−</sup>-to-NH<sub>3</sub> over Ni-BO<sub>x</sub>/NF are superior to those of NF along all applied potentials, delivering a record high FE of over 94% (Figure 3e). A <sup>15</sup>N-labeled NO<sub>3</sub><sup>−</sup> reduction experiment further confirmed the NH<sub>3</sub> synthesis from the reduction of NO<sub>3</sub><sup>−</sup> anions (Figure 3f).<sup>8,14</sup>

Furthermore, the electrochemical stability of the Ni-BO<sub>x</sub>/NF electrode for NO<sub>3</sub><sup>−</sup>-to-NH<sub>3</sub> conversion was evaluated over 30 cycles. As shown in Figure 3g, the values of FEs and NH<sub>3</sub> yield rates were not steady but were held together in tens of cycles. The Ni-BO<sub>x</sub>/NF electrode, after a 30-cycle test, can still provide a considerable NH<sub>3</sub> yield rate of 10.7 mg h<sup>−1</sup> cm<sup>−2</sup> and

an FE of 81.8%, significantly higher than the fresh NF electrode (7.5 mg h<sup>−1</sup> cm<sup>−2</sup> and 48.5% from Figure 3d,e) under identical conditions. We found that the slight performance loss was mainly due to surface oxidation and etching of B (Figure S16). We then implemented a second, simple boronization treatment for the spent Ni-BO<sub>x</sub>/NF electrode. The recycled electrode was fully restored to the original performance and enabled an increased NH<sub>3</sub> yield rate (22.5 mg h<sup>−1</sup> cm<sup>−2</sup> at the 33rd cycle) and stable FEs for nitrate reduction into ammonia. These results suggest that the Ni-BO<sub>x</sub>/NF electrode can be a promising candidate for industrial NO<sub>3</sub><sup>−</sup>-to-NH<sub>3</sub> conversions, paralleling or outpacing most previously reported earth-abundant electrocatalysts (Table 1).

**Mechanism.** We carried out *in situ* external reflection FTIR (see methods in the Supporting Information) to track the adsorbed species on the electrode surfaces of Ni-BO<sub>x</sub>/NF and NF during the electroreduction of NO<sub>3</sub><sup>−</sup> to NH<sub>3</sub>. In Figures 4a and S17, the upward adsorption bands in the ranges of 1500–1565 and 1662–1726 cm<sup>−1</sup> reveal \*NO<sub>3</sub> species,<sup>54,55</sup> verifying the consumption of NO<sub>3</sub><sup>−</sup> by the applied potential. The upward bands in 1610–1660 cm<sup>−1</sup> are attributed to the HOH bending ( $\delta$ HOH) mode of H<sub>2</sub>O,<sup>56</sup> implying the water electrolysis to deliver protons. Meanwhile, downward bands in 1735–1942 cm<sup>−1</sup> indicate the adsorption of \*NO species on the Ni surface.<sup>54,57</sup> The existence of \*NO<sub>2</sub> and \*NH<sub>2</sub> intermediates can be observed from the downward bands centered at 1292 and 1330 cm<sup>−1</sup>,<sup>54,58</sup> respectively. The downward adsorption bands in 1420–1490 cm<sup>−1</sup> further confirm the generation of NH<sub>3</sub> on the electrodes.<sup>59</sup> With the increase of potential from −0.5 to −1.5 V, the adsorption band position of the \*O–H bond gradually transferred to that of the \*N–H bond (Figure 4b) due to the nitrate hydrogenation,<sup>58,59</sup> and the sulfate (SO<sub>4</sub><sup>2−</sup>) was repelled from the surface by the formation of intermediates and NH<sub>3</sub> (Figure S18).

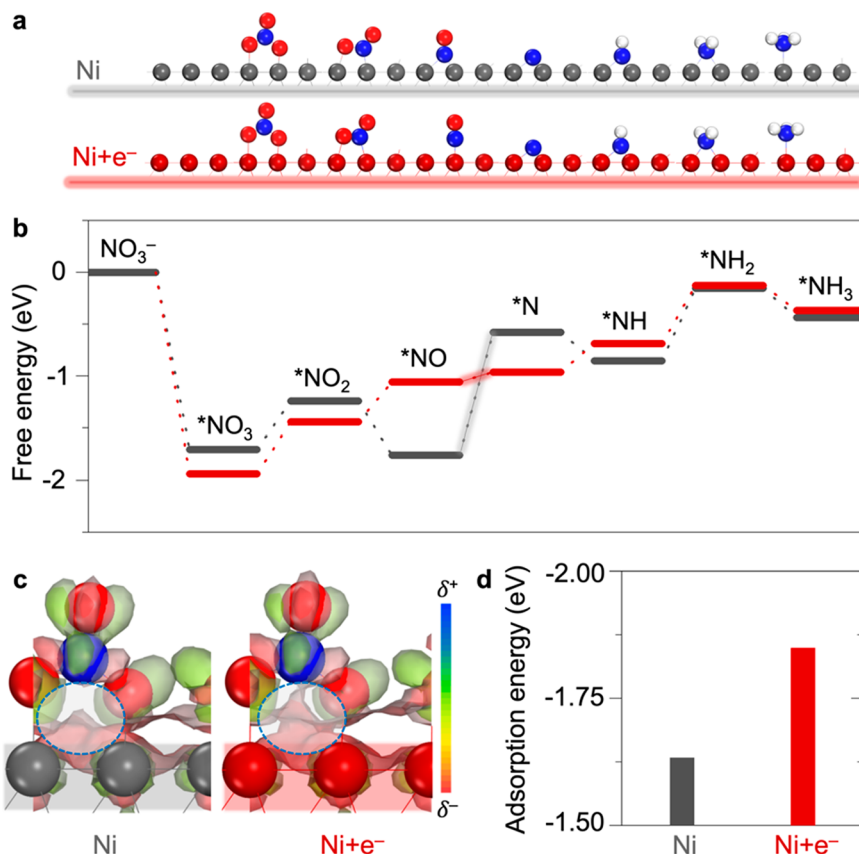


**Figure 5.** DFT calculations. (a) Optimized adsorption configurations and corresponding free energy diagram (b) for each step of the nitrate reduction process on neutral Ni and electron-abundant Ni ( $\text{Ni}+\text{e}^-$ ). White, red, and blue spheres represent H, O, and N atoms; gray and dark-washed red spheres correspond to neutral Ni and electron-abundant Ni atoms, respectively. (c) CDD stereograms after the adsorption of  $\text{NO}_3^-$  anion onto the Ni and  $\text{Ni}+\text{e}^-$  models and the corresponding calculated adsorption energies (d). Dotted ellipses in panel c are used to guide the eye.

In addition, the downward band at  $2077.0\text{ cm}^{-1}$  that appeared under  $-1.2\text{ V}$  could be attributed to the adsorption of  $^*\text{H}$  on the  $\text{Ni-BO}_x/\text{NF}$  electrode (Figure 4c).<sup>60,61</sup> It shifted to  $2072.2\text{ cm}^{-1}$  under  $-1.5\text{ V}$ . The  $\text{Ni-BO}_x/\text{NF}$  thus yields a lower Stark turn rate of  $16.0\text{ cm}^{-1}\text{ V}^{-1}$  in comparison to that of NF (Figure 4d,  $21.2\text{ cm}^{-1}\text{ V}^{-1}$ ), indicating a weaker affinity of  $^*\text{H}$  over the  $\text{Ni-BO}_x/\text{NF}$  electrode. This result demonstrates that electron-abundant  $\text{Ni-BO}_x/\text{NF}$  decreases the otherwise strong absorption of  $^*\text{H}$  on the Ni surface. It thereby provides a controlled active site for promoting the hydrogenation of  $\text{NO}_3^-$ , while depressing the HER, and leads to a high selectivity for the electrochemical reduction of  $\text{NO}_3^-$  into  $\text{NH}_3$ .

Furthermore, we performed density functional theory (DFT) calculations to unveil the origin of the electron-abundant Ni surface in promoting the electrochemical reduction of nitrate into ammonia (Figure 5, and Methods in the Supporting Information). Combining with the in situ external reflection FTIR results in Figure 4, the  $\text{NO}_3^-$ -to- $\text{NH}_3$  reaction ( $\text{NO}_3^- (\text{aq}) + 9\text{H}^+(\text{aq}) + 8\text{e}^- \rightarrow \text{NH}_3(\text{g}) + 3\text{H}_2\text{O}(\text{l})$ ) was simulated through several deoxidation reactions followed by hydrogenation reactions to  $\text{NH}_3$  (Figure 5a,b), in line with literature reports.<sup>51</sup> The potential-dependent step (PDS) over the Ni(111) surface is found to be the deoxidation reaction of  $^*\text{NO}$  to  $^*\text{N}$  with a formation barrier of  $1.18\text{ eV}$ , which is largely depressed to  $0.10\text{ eV}$  by the addition of electrons to the Ni surface ( $\text{Ni}+\text{e}^-$  model). Moreover, PDS is converted as the hydrogenation reaction of  $^*\text{NH}$  to  $^*\text{NH}_2$  on the  $\text{Ni}+\text{e}^-$  model

with a lower formation barrier of  $0.56\text{ eV}$ , accounting for the more favorable electrochemical reaction kinetics over the electron-abundant Ni surface.

From the charge density difference (CDD) stereograms between absorbed  $\text{NO}_3^-$  and support models (Figure 5c), a more considerable electron accumulation (red) area can be observed over the  $\text{Ni}+\text{e}^-$  model, possibly due to the stronger electron coupling between the electron-abundant Ni surface and the delocalized  $\pi$  electrons surrounding the  $\text{NO}_3^-$  anions. The calculated adsorption energy of nitrate (Figure 5d) over the surface of the  $\text{Ni}+\text{e}^-$  model ( $-1.85\text{ eV}$ ) is thus more negative than that of Ni ( $-1.63\text{ eV}$ ), forcefully underpinning the ability of the electron-abundant  $\text{Ni-BO}_x/\text{NF}$  electrode in capturing the nitrate anions. In addition, the potentials of zero charge ( $E_z$ ) of NF and  $\text{Ni-BO}_x/\text{NF}$  electrodes can be approximately calculated as  $0.16$  and  $0.01\text{ eV}$  ( $E_z = \Phi - 5.01\text{ eV}$ ;  $\Phi$ : work function), respectively.<sup>62</sup> The lower anodic  $E_z$  value of  $\text{Ni-BO}_x/\text{NF}$  signifies that the electrode would provide less negatively charged surfaces and therefore limit electrostatically attracted protons,<sup>36</sup> leading to the prevention of surface  $\text{H}_2$  generation. The DFT calculations further reveal that the  $\text{Ni}+\text{e}^-$  surface has a smaller  $\Delta G_{\text{H}^*}$  absolute value than bare Ni (Figure S19), implying a lower HER activity over the  $\text{Ni-BO}_x/\text{NF}$  electrode. These results collectively reveal why the electron-abundant  $\text{Ni-BO}_x/\text{NF}$  electrode with lowered work function presents an elevated performance for  $\text{NO}_3^-$ -to- $\text{NH}_3$  conversion compared with bare NF.

In summary, we have introduced a simple and rapid boronization treatment to develop commercial nickel foam into a high-performance electrode for nitrate reduction into ammonia. The work function of nickel foam is decreased by converting surface nickel oxides into dyadic nanosheets through metallic Ni and amorphous nickel borate species, enabling electron-abundant Ni surfaces for capturing and rapidly transforming nitrate anions. Our electrodes can be used for tens of cycles and then readily recycled when exhausted by simply applying another round of boronization. We also conclude that our strategy of fabricating a targeted electrocatalytic surface with desired electronic properties for nitrate-to-ammonia conversion may provide direct design insights into developing highly efficient electrode materials with wide implications. Future efforts can be focused on utilizing this high-performance electrode in membrane reactors to convert nitrate into ammonia and in metal-nitrate battery assemblies to capitalize on abundant electron–proton flow, thus constructing more practical systems for environmental waste remediation and energy storage.

## ■ ASSOCIATED CONTENT

### § Supporting Information

The Supporting Information is available free of charge at <https://pubs.acs.org/doi/10.1021/acsenergylett.3c01139>.

Experimental section; DFT calculations; SEM; TEM; XRD; UPS, CV, UV-vis, NMR, XPS, *in situ* FTIR, and potential-independent chronoamperometry curves; detailed discussions ([PDF](#))

## ■ AUTHOR INFORMATION

### Corresponding Authors

Xin-Hao Li – School of Chemistry and Chemical Engineering, Frontiers Science Center for Transformative Molecules, Shanghai Jiao Tong University, Shanghai 200240, P. R. China; [orcid.org/0000-0003-1643-4631](https://orcid.org/0000-0003-1643-4631); Email: [xinhaoli@sjtu.edu.cn](mailto:xinhaoli@sjtu.edu.cn)

Cafer T. Yavuz – Oxide & Organic Nanomaterials for Energy & Environment (ONE) Laboratory, Advanced Membranes & Porous Materials (AMPM) Center, and KAUST Catalysis Center (KCC), Physical Science & Engineering (PSE), King Abdullah University of Science and Technology (KAUST), Thuwal 23955, Saudi Arabia; [orcid.org/0000-0003-0580-3331](https://orcid.org/0000-0003-0580-3331); Email: [cafer.yavuz@kaust.edu.sa](mailto:cafer.yavuz@kaust.edu.sa)

### Authors

Zhong-Hua Xue – Oxide & Organic Nanomaterials for Energy & Environment (ONE) Laboratory, Advanced Membranes & Porous Materials (AMPM) Center, and KAUST Catalysis Center (KCC), Physical Science & Engineering (PSE), King Abdullah University of Science and Technology (KAUST), Thuwal 23955, Saudi Arabia; Department of Applied Chemistry, School of Science, Anhui Agricultural University, Hefei 230036, P. R. China

Han-Cheng Shen – Department of Applied Chemistry, School of Science, Anhui Agricultural University, Hefei 230036, P. R. China

Peirong Chen – Department of Applied Chemistry, School of Science, Anhui Agricultural University, Hefei 230036, P. R. China

Guang-Xue Pan – Department of Applied Chemistry, School of Science, Anhui Agricultural University, Hefei 230036, P. R. China

Wei-Wei Zhang – Department of Applied Chemistry, School of Science, Anhui Agricultural University, Hefei 230036, P. R. China

Wei-Meng Zhang – Department of Applied Chemistry, School of Science, Anhui Agricultural University, Hefei 230036, P. R. China

Shi-Nan Zhang – School of Chemistry and Chemical Engineering, Frontiers Science Center for Transformative Molecules, Shanghai Jiao Tong University, Shanghai 200240, P. R. China

Complete contact information is available at:  
<https://pubs.acs.org/10.1021/acsenergylett.3c01139>

### Author Contributions

<sup>†</sup>Z.-H.X. and H.-C.S. contributed equally.

### Notes

The authors declare no competing financial interest.

## ■ ACKNOWLEDGMENTS

This work was financially supported by the King Abdullah University of Science and Technology (KAUST), the National Natural Science Foundation of China (22105002 and 22071146), Anhui Agricultural University (rc382003), Shanghai Science and Technology Committee (20520711600), and the SJTU-MPI partner group.

## ■ REFERENCES

- (1) Canfield, D. E.; Glazer, A. N.; Falkowski, P. G. The evolution and future of earth's nitrogen cycle. *Science* **2010**, *330*, 192–196.
- (2) Duca, M.; Koper, M. T. M. Powering denitrification: the perspectives of electrocatalytic nitrate reduction. *Energy Environ. Sci.* **2012**, *5* (12), 9726–9742.
- (3) Montoya, J. H.; Tsai, C.; Vojvodic, A.; Nørskov, J. K. The challenge of electrochemical ammonia synthesis: A new perspective on the role of nitrogen scaling relations. *ChemSusChem* **2015**, *8* (13), 2180–2186.
- (4) Chen, J. G.; Crooks, R. M.; Seefeldt, L. C.; Bren, K. L.; Bullock, R. M.; Darenbourg, M. Y.; Holland, P. L.; Hoffman, B.; Janik, M. J.; Jones, A. K.; et al. Beyond fossil fuel-driven nitrogen transformations. *Science* **2018**, *360* (6391), No. eaar6611.
- (5) Xu, S.; Ashley, D. C.; Kwon, H. Y.; Ware, G. R.; Chen, C. H.; Losovyj, Y.; Gao, X.; Jakubikova, E.; Smith, J. M. A flexible, redox-active macrocycle enables the electrocatalytic reduction of nitrate to ammonia by a cobalt complex. *Chem. Sci.* **2018**, *9* (22), 4950–4958.
- (6) Guo, W.; Zhang, K.; Liang, Z.; Zou, R.; Xu, Q. Electrochemical nitrogen fixation and utilization: theories, advanced catalyst materials and system design. *Chem. Soc. Rev.* **2019**, *48* (24), 5658–5716.
- (7) Li, J.; Li, M.; An, N.; Zhang, S.; Song, Q.; Yang, Y.; Liu, X. Atomically dispersed Fe atoms anchored on S and N-codoped carbon for efficient electrochemical denitrification. *Proc. Natl. Acad. Sci. U. S. A.* **2021**, *118* (33), No. e2105628118.
- (8) Gao, P.; Xue, Z. H.; Zhang, S. N.; Xu, D.; Zhai, G. Y.; Li, Q. Y.; Chen, J. S.; Li, X. H. Schottky barrier-induced surface electric field boosts universal reduction of  $\text{NO}_x^-$  in water to ammonia. *Angew. Chem., Int. Ed.* **2021**, *60* (38), 20711–20716.
- (9) Garcia-Segura, S.; Lanzarini-Lopes, M.; Hristovski, K.; Westerhoff, P. Electrocatalytic reduction of nitrate: Fundamentals to full-scale water treatment applications. *Appl. Catal. B Environ.* **2018**, *236*, 546–568.
- (10) McEnaney, J. M.; Blair, S. J.; Nielander, A. C.; Schwalbe, J. A.; Koshy, D. M.; Cargnello, M.; Jaramillo, T. F. Electrolyte engineering for efficient electrochemical nitrate reduction to ammonia on a

- titanium electrode. *ACS Sustainable Chem. Eng.* **2020**, *8* (7), 2672–2681.
- (11) Zhang, H.; Wang, C.; Luo, H.; Chen, J.; Kuang, M.; Yang, J. Iron nanoparticles protected by chainmail-structured graphene for durable electrocatalytic nitrate reduction to nitrogen. *Angew. Chem., Int. Ed.* **2023**, *62* (5), No. e202217071.
- (12) Rosca, V.; Duca, M.; de Groot, M. T.; Koper, M. T. M. Nitrogen cycle electrocatalysis. *Chem. Rev.* **2009**, *109*, 2209–2244.
- (13) Chen, G.-F.; Yuan, Y.; Jiang, H.; Ren, S.-Y.; Ding, L.-X.; Ma, L.; Wu, T.; Lu, J.; Wang, H. Electrochemical reduction of nitrate to ammonia via direct eight-electron transfer using a copper-molecular solid catalyst. *Nat. Energy* **2020**, *5* (8), 605–613.
- (14) Chen, F. Y.; Wu, Z. Y.; Gupta, S.; Rivera, D. J.; Lambeets, S. V.; Pecaut, S.; Kim, J. Y. T.; Zhu, P.; Finfrock, Y. Z.; Meira, D. M.; et al. Efficient conversion of low-concentration nitrate sources into ammonia on a Ru-dispersed Cu nanowire electrocatalyst. *Nat. Nanotechnol.* **2022**, *17* (7), 759–767.
- (15) He, W.; Zhang, J.; Dieckhofer, S.; Varhade, S.; Brix, A. C.; Lielpetere, A.; Seisel, S.; Junqueira, J. R. C.; Schuhmann, W. Splicing the active phases of copper/cobalt-based catalysts achieves high-rate tandem electroreduction of nitrate to ammonia. *Nat. Commun.* **2022**, *13* (1), 1129.
- (16) Xue, Z. H.; Zhang, S. N.; Lin, Y. X.; Su, H.; Zhai, G. Y.; Han, J. T.; Yu, Q. Y.; Li, X. H.; Antonietti, M.; Chen, J. S. Electrochemical reduction of  $\text{N}_2$  into  $\text{NH}_3$  by donor-acceptor couples of Ni and Au nanoparticles with a 67.8% faradaic efficiency. *J. Am. Chem. Soc.* **2019**, *141*, 14976–14980.
- (17) van Langevelde, P. H.; Katsounaros, I.; Koper, M. T. M. Electrocatalytic nitrate reduction for sustainable ammonia production. *Joule* **2021**, *5* (2), 290–294.
- (18) Zhao, X.; Zhu, Z.; He, Y.; Zhang, H.; Zhou, X.; Hu, W.; Li, M.; Zhang, S.; Dong, Y.; Hu, X.; et al. Simultaneous anchoring of Ni nanoparticles and single-atom Ni on BCN matrix promotes efficient conversion of nitrate in water into high-value-added ammonia. *Chem. Eng. J.* **2022**, *433*, 133190.
- (19) Cai, J.; Wei, Y.; Cao, A.; Huang, J.; Jiang, Z.; Lu, S.; Zang, S.-Q. Electrocatalytic nitrate-to-ammonia conversion with ~ 100% Faradaic efficiency via single-atom alloying. *Appl. Catal. B Environ.* **2022**, *316*, 121683.
- (20) Xu, H.; Ma, Y.; Chen, J.; Zhang, W. X.; Yang, J. Electrocatalytic reduction of nitrate - a step towards a sustainable nitrogen cycle. *Chem. Soc. Rev.* **2022**, *51* (7), 2710–2758.
- (21) Li, J.; Zhan, G.; Yang, J.; Quan, F.; Mao, C.; Liu, Y.; Wang, B.; Lei, F.; Li, L.; Chan, A. W. M.; et al. Efficient ammonia electrosynthesis from nitrate on strained ruthenium nanoclusters. *J. Am. Chem. Soc.* **2020**, *142* (15), 7036–7046.
- (22) Liu, H.; Lang, X.; Zhu, C.; Timoshenko, J.; Ruscher, M.; Bai, L.; Guijarro, N.; Yin, H.; Peng, Y.; Li, J.; et al. Efficient electrochemical nitrate reduction to ammonia with copper-supported rhodium cluster and single-atom catalysts. *Angew. Chem., Int. Ed.* **2022**, *61* (23), No. e202202556.
- (23) Guo, Y.; Zhang, R.; Zhang, S.; Zhao, Y.; Yang, Q.; Huang, Z.; Dong, B.; Zhi, C. Pd doping-weakened intermediate adsorption to promote electrocatalytic nitrate reduction on  $\text{TiO}_2$  nanoarrays for ammonia production and energy supply with zinc-nitrate batteries. *Energy Environ. Sci.* **2021**, *14* (7), 3938–3944.
- (24) Jiang, M.; Su, J.; Song, X.; Zhang, P.; Zhu, M.; Qin, L.; Tie, Z.; Zuo, J. L.; Jin, Z. Interfacial reduction nucleation of noble metal nanodots on redox-active metal-organic frameworks for high-efficiency electrocatalytic conversion of nitrate to ammonia. *Nano Lett.* **2022**, *22* (6), 2529–2537.
- (25) Zhai, G.-Y.; Li, Q.-Y.; Zhang, S.-N.; Xu, D.; Xia, S.-Y.; Gao, P.; Lin, X.; Lin, Y.-X.; Cheng, J.-H.; Hu, W.-Y.; et al. Accelerating the activation of  $\text{NO}_x^-$  on Ru nanoparticles for ammonia production by tuning their electron deficiency. *CCS Chem.* **2022**, *4* (11), 3455–3462.
- (26) Han, S.; Li, H.; Li, T.; Chen, F.; Yang, R.; Yu, Y.; Zhang, B. Ultralow overpotential nitrate reduction to ammonia via a three-step relay mechanism. *Nat. Catal.* **2023**, *6*, 402–414.
- (27) Wu, Z. Y.; Karamad, M.; Yong, X.; Huang, Q.; Cullen, D. A.; Zhu, P.; Xia, C.; Xiao, Q.; Shakouri, M.; Chen, F. Y.; et al. Electrochemical ammonia synthesis via nitrate reduction on Fe single atom catalyst. *Nat. Commun.* **2021**, *12* (1), 2870.
- (28) Li, J.; Li, M.; An, N.; Zhang, S.; Song, Q.; Yang, Y.; Li, J.; Liu, X. Boosted ammonium production by single cobalt atom catalysts with high Faradic efficiencies. *Proc. Natl. Acad. Sci. U. S. A.* **2022**, *119* (29), No. e2123450119.
- (29) Zhang, R.; Guo, Y.; Zhang, S.; Chen, D.; Zhao, Y.; Huang, Z.; Ma, L.; Li, P.; Yang, Q.; Liang, G.; et al. Efficient ammonia electrosynthesis and energy conversion through a Zn-nitrate battery by iron doping engineered nickel phosphide catalyst. *Adv. Energy Mater.* **2022**, *12* (13), 2103872.
- (30) Xu, Y.-T.; Ren, K.-C.; Tao, Z.-M.; Sam, D. K.; Feng, E.; Wang, X.; Zhang, G.; Wu, J.; Cao, Y. A new catalyst based on disposed red mud for the efficient electrochemical reduction of nitrate-to-ammonia. *Green Chem.* **2023**, *25* (2), 589–595.
- (31) Fan, X.; Xie, L.; Liang, J.; Ren, Y.; Zhang, L.; Yue, L.; Li, T.; Luo, Y.; Li, N.; Tang, B.; et al. In situ grown  $\text{Fe}_3\text{O}_4$  particle on stainless steel: A highly efficient electrocatalyst for nitrate reduction to ammonia. *Nano Res.* **2022**, *15* (4), 3050–3055.
- (32) Ford, C. L.; Park, Y. J.; Matson, E. M.; Gordon, Z.; Fout, A. R. A bioinspired iron catalyst for nitrate and perchlorate reduction. *Science* **2016**, *354*, 741–743.
- (33) Li, L.; Tang, C.; Cui, X.; Zheng, Y.; Wang, X.; Xu, H.; Zhang, S.; Shao, T.; Davey, K.; Qiao, S. Z. Efficient nitrogen fixation to ammonia through integration of plasma oxidation with electrocatalytic reduction. *Angew. Chem., Int. Ed.* **2021**, *60* (25), 14131–14137.
- (34) Chen, L.; Xu, Q.; Oener, S. Z.; Fabrizio, K.; Boettcher, S. W. Design principles for water dissociation catalysts in high-performance bipolar membranes. *Nat. Commun.* **2022**, *13* (1), 3846.
- (35) Sanchis, I.; Diaz, E.; Pizarro, A. H.; Rodriguez, J. J.; Mohedano, A. F. Nitrate reduction with bimetallic catalysts. A stability-addressed overview. *Sep. Purif. Technol.* **2022**, *290*, 120750.
- (36) Carvalho, O. Q.; Marks, R.; Nguyen, H. K. K.; Vitale-Sullivan, M. E.; Martinez, S. C.; Arnadottir, L.; Stoerzinger, K. A. Role of electronic structure on nitrate reduction to ammonium: A periodic journey. *J. Am. Chem. Soc.* **2022**, *144* (32), 14809–14818.
- (37) Wang, Y.; Xu, A.; Wang, Z.; Huang, L.; Li, J.; Li, F.; Wicks, J.; Luo, M.; Nam, D. H.; Tan, C. S.; et al. Enhanced nitrate-to-ammonia activity on copper-nickel alloys via tuning of intermediate adsorption. *J. Am. Chem. Soc.* **2020**, *142* (12), 5702–5708.
- (38) Lv, X.; Mou, T.; Li, J.; Kou, L.; Frauenheim, T. Tunable surface chemistry in heterogeneous bilayer single-atom catalysts for electrocatalytic  $\text{NO}_x$  reduction to ammonia. *Adv. Funct. Mater.* **2022**, *32* (28), 2201262.
- (39) Yang, J.; Qi, H.; Li, A.; Liu, X.; Yang, X.; Zhang, S.; Zhao, Q.; Jiang, Q.; Su, Y.; Zhang, L.; et al. Potential-driven restructuring of Cu single atoms to nanoparticles for boosting the electrochemical reduction of nitrate to ammonia. *J. Am. Chem. Soc.* **2022**, *144* (27), 12062–12071.
- (40) Babar, P.; Mahmood, J.; Maligal-Ganesh, R. V.; Kim, S.-J.; Xue, Z.; Yavuz, C. T. Electronic structure engineering for electrochemical water oxidation. *J. Mater. Chem. A* **2022**, *10* (38), 20218–20241.
- (41) Xue, Z. H.; Su, H.; Yu, Q. Y.; Zhang, B.; Wang, H. H.; Li, X. H.; Chen, J. S. Janus Co/CoP nanoparticles as efficient Mott-Schottky electrocatalysts for overall water splitting in wide pH range. *Adv. Energy Mater.* **2017**, *7* (12), 1602355.
- (42) Wang, H.; Song, A. J.; Chen, H.; Zhang, W. M.; Xue, Z. H. Charge-storage nickel substrate-boosted  $\text{CuP}_2$  nanosheet for the electrochemical oxygen evolution reaction. *Inorg. Chem.* **2022**, *61* (32), 12489–12493.
- (43) Babar, P.; Patil, K.; Mahmood, J.; Kim, S.-j.; Kim, J. H.; Yavuz, C. T. Low-overpotential overall water splitting by a cooperative interface of cobalt-iron hydroxide and iron oxyhydroxide. *Cell Rep. Phys. Sci.* **2022**, *3* (2), 100762.
- (44) Xue, Z.-H.; Han, J.-T.; Feng, W.-J.; Yu, Q.-Y.; Li, X.-H.; Antonietti, M.; Chen, J.-S. Tuning the adsorption energy of methanol molecules along Ni-N-doped carbon phase boundaries by the Mott-

- Schottky effect for gas-phase methanol dehydrogenation. *Angew. Chem., Int. Ed.* **2018**, *57* (10), 2697–2701.
- (45) Zhang, P.; Wang, L.; Yang, S.; Schott, J. A.; Liu, X.; Mahurin, S. M.; Huang, C.; Zhang, Y.; Fulvio, P. F.; Chisholm, M. F.; et al. Solid-state synthesis of ordered mesoporous carbon catalysts via a mechanochemical assembly through coordination cross-linking. *Nat. Commun.* **2017**, *8*, 15020.
- (46) Murphy, D. W.; Zahurak, S. M.; Vyas, B.; Thomas, M.; Badding, M. E.; Fang, W. C. A new route to metal hydrides. *Chem. Mater.* **1993**, *5*, 767–769.
- (47) Chen, P.; Xu, K.; Zhou, T.; Tong, Y.; Wu, J.; Cheng, H.; Lu, X.; Ding, H.; Wu, C.; Xie, Y. Strong-coupled cobalt borate nanosheets/graphene hybrid as electrocatalyst for water oxidation under both alkaline and neutral conditions. *Angew. Chem., Int. Ed.* **2016**, *55* (7), 2488–2492.
- (48) Guo, F.; Wu, Y.; Chen, H.; Liu, Y.; Yang, L.; Ai, X.; Zou, X. High-performance oxygen evolution electrocatalysis by boronized metal sheets with self-functionalized surfaces. *Energy Environ. Sci.* **2019**, *12* (2), 684–692.
- (49) Jiang, W. J.; Niu, S.; Tang, T.; Zhang, Q. H.; Liu, X. Z.; Zhang, Y.; Chen, Y. Y.; Li, J. H.; Gu, L.; Wan, L. J.; et al. Crystallinity-modulated electrocatalytic activity of a nickel(II) borate thin layer on Ni<sub>3</sub>B for efficient water oxidation. *Angew. Chem., Int. Ed.* **2017**, *56* (23), 6572–6577.
- (50) Wang, J.; Wu, D.; Li, M.; Wei, X.; Yang, X.; Shao, M.; Gu, M. Bismuth ferrite as an electrocatalyst for the electrochemical nitrate reduction. *Nano Lett.* **2022**, *22* (13), 5600–5606.
- (51) Zhang, S.; Li, M.; Li, J.; Song, Q.; Liu, X. High-ammonia selective metal-organic framework-derived Co-doped Fe/Fe<sub>2</sub>O<sub>3</sub> catalysts for electrochemical nitrate reduction. *Proc. Natl. Acad. Sci. U. S. A.* **2022**, *119* (6), No. e2115504119.
- (52) Wang, Y. M.; Cai, J.; Wang, Q. Y.; Li, Y.; Han, Z.; Li, S.; Gong, C. H.; Wang, S.; Zang, S. Q.; Mak, T. C. W. Electropolymerization of metal clusters establishing a versatile platform for enhanced catalysis performance. *Angew. Chem., Int. Ed.* **2022**, *61* (10), No. e202114538.
- (53) Ren, T.; Yu, Z.; Yu, H.; Deng, K.; Wang, Z.; Li, X.; Wang, H.; Wang, L.; Xu, Y. Interfacial polarization in metal-organic framework reconstructed Cu/Pd/CuO<sub>x</sub> multi-phase heterostructures for electrocatalytic nitrate reduction to ammonia. *Appl. Catal. B Environ.* **2022**, *318*, 121805.
- (54) Szanyi, J.; Kwak, J. H.; Zhu, H.; Peden, C. H. Characterization of Cu-SSZ-13 NH<sub>3</sub> SCR catalysts: an *in situ* FTIR study. *Phys. Chem. Chem. Phys.* **2013**, *15* (7), 2368–2380.
- (55) Kunov-Kruse, A. J.; Thomassen, P. L.; Riisager, A.; Mossin, S.; Fehrmann, R. Absorption and oxidation of nitrogen oxide in ionic liquids. *Chem.—Eur. J.* **2016**, *22* (33), 11745–11755.
- (56) Ataka, K.; Yotsuyanagi, T.; Osawa, M. Potential-dependent reorientation of water molecules at an electrode/electrolyte interface studied by surface-enhanced infrared absorption spectroscopy. *J. Phys. Chem.* **1996**, *100*, 10664–10672.
- (57) Mihaylov, M.; Hadjiivanov, K. FTIR study of CO and NO adsorption and coadsorption on Ni-ZSM-5 and Ni/SiO<sub>2</sub>. *Langmuir* **2002**, *18*, 4376–4383.
- (58) Ren, J.-T.; Wan, C.-Y.; Pei, T.-Y.; Lv, X.-W.; Yuan, Z.-Y. Promotion of electrocatalytic nitrogen reduction reaction on N-doped porous carbon with secondary heteroatoms. *Appl. Catal. B Environ.* **2020**, *266*, 118633.
- (59) Song, P.; Kang, L.; Wang, H.; Guo, R.; Wang, R. Nitrogen (N), phosphorus (P)-codoped porous carbon as a metal-free electrocatalyst for N<sub>2</sub> reduction under ambient conditions. *ACS Appl. Mater. Interfaces* **2019**, *11* (13), 12408–12414.
- (60) Fang, J. Y.; Zheng, Q. Z.; Lou, Y. Y.; Zhao, K. M.; Hu, S. N.; Li, G.; Akdim, O.; Huang, X. Y.; Sun, S. G. Ampere-level current density ammonia electrochemical synthesis using CuCo nanosheets simulating nitrite reductase bifunctional nature. *Nat. Commun.* **2022**, *13* (1), 7899.
- (61) Yao, Y.; Zhu, S.; Wang, H.; Li, H.; Shao, M. A spectroscopic study on the nitrogen electrochemical reduction reaction on gold and platinum surfaces. *J. Am. Chem. Soc.* **2018**, *140* (4), 1496–1501.
- (62) Trasatti, S. Work function, electronegativity, and electrochemical behaviour of metals: II. potentials of zero charge and “electrochemical” work functions. *J. Electroanal. Chem. Interface Electrochem.* **1971**, *33*, 351–378.